Stochastic radiative transfer in random media. II. Coupling of radiation to material

Cong-Zhang Gao ●,[*,†] Ying Cai,[†] Cun-Bo Zhang, Zhen-Ying Hong, Zheng-Feng Fan,[‡] Pei Wang,[§] and Jian-Guo Wang
Institute of Applied Physics and Computational Mathematics, Beijing 100088, People's Republic of China

We study the mechanism of the impact of random media on the stochastic radiation transport based on a one-dimensional (1D) planar model. To this end, we use a random sampling of mixtures combined with a deterministic solution of the time-dependent radiation transport equation coupled to a material temperature equation. Compared to purely absorbing cases [C.-Z. Gao *et al.*, Phys. Rev. E **102**, 022111 (2020)], we find that material temperatures can significantly suppress the impact of mixing distribution and size, which is understood from the analysis of energy transport channels. By developing a steady-state stochastic transport model, it is found that the mechanism of transmission of radiation is distance dependent, which is closely related to the mean free path of photons l_p. Furthermore, we suggest that it is the relationship between l_p and L (the width of random medium) that determines the impact of random media on the stochastic radiation transport, which is further corroborated by additional simulations. Most importantly, combining the proposed simple relationship and 1D simulations, we resolve the existing disputable issue of the impact of random media in previous multidimensional works, showing that multidimensional results are essentially consistent and the observed weak or remarkable impact of random media is mainly due to the distinctly different relationship between l_p and L. Our results may have practical implications in relevant experiments of stochastic radiative transfer.

I. INTRODUCTION

In recent decades, the interest in studying the transport of radiation in random media [1] has been persistently growing in a broad range of research fields such as astrophysics [2–4], plasma physics [5–7], reactor physics [8–11], and atmospheric science [12–14]; for reviews, see Refs. [15–17]. The resolution of radiation transport in random media in principle requires dealing with stochastic radiation transport equations, since the composition of random media is only known statistically by the volume fraction (or mixing probability) at a specified position at any time [18]. The statistical nature of random media's geometry adds more degrees of freedom (i.e., mixing distribution, size, and probability) to the background material with which photons interact, which enormously complicates the analysis of radiation transport process, in contrast to that in a homogeneous medium where the transport coefficients are typically deterministic and constant [18–20], i.e., independent of the spatial variable.

Among the extensive studies on this subject, a majority of theoretical works have focused on steady-state or time-independent stochastic radiative transfer [21–31], particularly in a binary random medium of two immiscible materials stochastically admixed, and a wealth of benchmark results have been presented in one-dimensional (1D) rod and planar geometries [24,26–29,31]. Recently, Larmier *et al.* [32–34] provided intense benchmark results for two- and three-dimensional cases. However, almost all of them have

treated the problem with nonparticipating materials, i.e., in the absence of material temperature, and the results may be inapplicable in the case of strong radiation heating the random media up to appreciable temperatures, which are typically the physical scenario in related practical applications. For example, in inertial confinement fusion (ICF) mixed layers of very different materials (e.g., low-Z gas admixed with ablator materials doped by high-Z dopants) interact intensively with driving energetic x rays in the phase of implosion and compression [35–37]. Under such circumstances, the radiation is strong enough and the random mixtures remain hot and dense, thus necessitating modeling the radiation transport in random media, taking into account the coupling of strong radiation to hot matter, which might be instructive in ICF simulations [5].

In relation to stochastic radiative transfer in participating random media (i.e., feedback due to the material is considered in radiation transport), a number of theoretical studies have been reported in both time-independent and time-dependent domains. In the time-independent condition, Vanderhaegen [22] considered the stochastic radiative transfer in a heterogeneous two-temperature medium, in which the temperature of respective materials was assumed to be known and unchanged by the radiation. For infinitely large distances with zero incident radiation, Vanderhaegen presented an analytical expression of the ensemble-averaged transmission, which was further simplified to a more compact form by assuming that the correlation length converged to zero. Nevertheless, Vanderhaegen also claimed that the model might be invalid in nonequilibrium situations.

In the time-dependent condition, Miller *et al.* [38] reported benchmark calculations for transport of radiation coupled to material in one-dimensional (1D) planar geometry binary random media using Markov mixing statistics, which

---
[*]czgao88@hotmail.com
[†]These authors contributed equally to this work.
[‡]fan_zhengfeng@iapcm.ac.cn
[§]wangpei@iapcm.ac.cn

have been explicitly compared to three approximate models by varying mixing sizes. Their numerical results showed that the Su-Pomraning model [39] was superior to both the Levermore-Pomraning and atomic mix models [18]. In a subsequent work, Prinja and Olson [40] developed reduced transport models for the ensemble-averaged radiation intensity and material energy density, which excluded the stochasticity of random geometry; the validity of these models has been carefully verified in numerical calculations over a wide range of model parameters. In recent decades, radiative transfer in participating random media has been extended to more sophisticated situations [41–47], i.e., in two and three dimensions, which have significantly improved our understanding of stochastic radiative transfer in realistic physical scenarios. From a comparative analysis of the aforementioned studies, it can readily be seen that more attention has been paid to establish approximate deterministic models via effective opacities or more accurate closures and to develop an efficient numerical algorithm to fully simulate stochastic radiation transport than to the influence of the random medium itself on radiation transport.

From a practical point of view, the knowledge of the impact of the properties of random media on stochastic radiation transport is crucial to manipulating the radiation flux through the random media. For instance, previous radiation transport experiments in inhomogeneous foam-Au plasmas [6,7] showed that the size of random mixtures can strongly affect the propagation of radiation-driven heat. Therefore, it is important, from a theoretical perspective, to elucidate the dependence of stochastic radiation transport on random media. In this context, based on a low-order angular approximation to radiation transport equations (the so-called $P_{1/3}$ equations), Olson carried out 2D simulations [41] and found that different mixing sizes weakly affected the radiation flux. By comparing the constant mixing distributions with exponential ones, a similar weak dependence on mixing distributions was also observed. When coupled to the material equation, Olson obtained nearly identical results for very different mixing distributions and sizes. Moreover, in a follow-up study in three dimensions, Olson [44] again confirmed different mixing distributions having little effect on radiation energy densities. Additionally, Brantley and Martos studied the same problem but without material temperature coupling in three dimensions using a Monte Carlo technique [48]. Basically, they found a remarkable dependence of the radiation of transmission and reflection on the mixing sizes and probabilities and a weak effect of mixing distributions. In Ref. [48] Brantley and Martos also claimed that their benchmark results were to some extent in contrast to those reported by Olson [41]. In other words, there is far from conclusive agreement on whether or not the properties of random media considerably affect the radiation transport, not to mention the underlying mechanism.

In order to better understand the discrepancy in multidimensions, in this paper we employ the 1D slab geometry model to perform a comprehensive and thorough study. One may argue that results obtained from the 1D slab geometry are different from those in multidimensions [41], but the relative magnitude of the impact of the properties of random media may not be strongly dependent on the dimensionality of stochastic mixtures. Compared to 2D and 3D calculations,

the 1D slab geometry in the present study is simple enough, but photon transport does occur in three dimensions by assuming translational invariance in the x and y dimensions. On the other hand, as we use the simplest nontrivial model for radiation transport, it is possible to establish the analytic physical model to interpret the numerical data, which may be difficult for multidimensional simulations. Most importantly, a systematic study on radiation transport in two and three dimensions in a wide range of parameters is computationally demanding, but it is more feasible in one dimension in the present work.

In this work, our goal is to figure out the mechanism of the impact of random media on stochastic radiation transport using a 1D slab model. We start by showing how the ensemble-averaged observables, e.g., the transmission of radiation, are systematically affected by random media in the presence of radiation-material coupling and examining to what extent the findings observed in pure absorbing cases [31] are applicable. Then we analyze the role of material temperature in stochastic radiative transfer by building a steady-state stochastic transport model and discuss the underlying mechanism of the impact of random media. Finally, we combine the proposed mechanism and 1D simulations to interpret previous multidimensional results, aiming to resolve the existing disputable issue of the impact of a random medium in previous works. As such, the present study can also be considered as an extension of our recent work in the regime of pure absorbing [31] into the time domain and participating random media.

The organization of the article is as follows. Section II presents a description of the theoretical model and key parameters. The present models are explicitly validated by previous benchmark results. Systematic results are presented in Sec. III, followed by a discussion of the role of material temperature and an analysis of the mechanism of the impact of random media in Sec. IV. Based on the proposed mechanism and 1D simulations, we interpret self-consistently previous multidimensional results in Sec. V. We summarize, draw conclusions, and offer perspective for future work in Sec. VI.

II. THEORETICAL METHOD

In order to obtain reliable and robust results on radiation transport through a layered binary stochastic mixture, we use a benchmark procedure involving three main steps to evaluate the ensemble-averaged transport results of interest, as described in Refs. [24,26,27,29,31]. First, a number of physical realizations of the layered stochastic mixture are randomly sampled from the mixing distribution for the given mixing probabilities. Second, in each sample the radiation transport equations coupled to the material temperature equations are deterministically solved and the transport results are recorded. Third, ensemble-averaged results are naturally obtained.

A. Model description

Figure 1 schematically shows a typical physical realization (side view), which occupies the spatial domain $\{-\infty < x < \infty, -\infty < y < \infty, 0 \leqslant z \leqslant L\}$. It consists of alternating materials 1 and 2 with random thicknesses in the z direction,
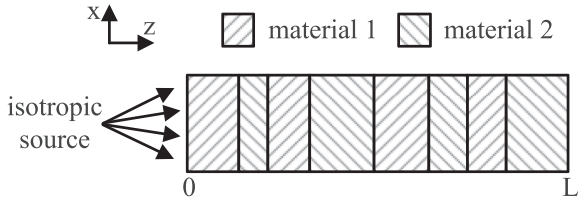
FIG. 1. Schematic of a physical realization of a binary random medium in the planar geometry. Materials 1 and 2 are labeled by different patterns. The total width of the random medium is denoted by L. The isotropic radiation source is placed at the left material surface.

which is also referred to as the slab geometry [19,49,50]. The algorithm of the random sampling of such stochastic mixtures, based on the chord length distribution (CLD), can be found in Refs. [24,26,27,29,31]. An isotropic radiation source at the given temperature presents at $z = 0$ (the left boundary) and zero incident intensity is considered at $z = L$ (the right boundary), which constitutes the initial boundary condition of the problem.

Once the sampling of mixtures is completed, the deterministic method is applied for the given physical realization to solve the radiation-material coupled transport equations and to average the transport quantities of interest over a number of random samplings. Conventionally, photon transport occurs in three dimensions in any physical realization of mixtures, which can be described by three spatial variables (x, y, and z), one energy variable (E), two angular variables (a polar angle θ and an azimuthal angle ϕ), and one temporal variable (t) [18,19]. In the present work, we assume that the physical parameters such as opacity are spatially uniform, i.e., independent of x and y. With appropriate initial and boundary conditions that are only z dependent, it is thus reduced to a 1D problem depending on the z coordinate. For the slab geometry, we consider here the monoenergetic, purely absorbing, source-free photon transport coupled to material temperature; therefore, a standard description [18,51] for the specific radiation intensity ψ requires one temporal (t), one spatial (z), and one angular (θ) variable, and for the material energy density it necessitates one temporal (t) and one spatial (z) variable. In this context, the coupled equations can be written as [18]

$$\frac{1}{c}\frac{\partial}{\partial t}\psi(t, z, \mu) + \mu\frac{\partial}{\partial z}\psi(t, z, \mu) + \sigma_a\psi(t, z, \mu)$$
$$= \frac{c\sigma_a}{2}\phi(t, z),$$
$$\frac{\partial}{\partial t}\phi(t, z) = -c\sigma_a\phi(t, z) + \sigma_a\int_{-1}^{1}d\mu'\psi(t, z, \mu'), \quad (1)$$

where $\psi(t, z, \mu)$ denotes the time- and angle-dependent specific radiation intensity and $\phi(t, z)$ the time-dependent material energy density, given that it is at position z. The speed of light in vacuum is denoted by c (=2.9979 × 10^{-2} cm/ps), and μ signifies the cosine of the angle between the z axis and the photon propagation direction, i.e., $\mu = \cos\theta$. In addition, σ_a is the absorption opacity in units of cm^{-1}, which is invariable in time but not in space for a binary stochastic mixture. For

simplicity, the value of absorption opacity is fixed and thus we will not be considering temperature-dependent opacities in this work.

Equations (1) can be briefly explained as follows. (a) It should be emphasized that we have used $\phi(t, z) = aT^4(t, z)$, where T is the time-varying local material's temperature at position z in units of keV and a is the radiation constant (=1.37 × 10^{-5} J cm^{-3} eV^{-4}), which allows us to obtain two coupled but linear equations. (b) Equations (1) describe the absorption-emission process of photon transport through stochastic mixtures. Inclusion of the photons' scattering is straightforward, but we have purposely ignored it, since the existence of the scattering term will certainly complicate the analysis. (c) For a fixed point z in a given physical realization, the same material is found for all times, i.e., material transitions are neglected in time, and this assumption has been widely used in previous benchmark studies of stochastic radiative transfer [24,26–29,31,38].

To simulate a binary stochastic mixture, we build a large ensemble of physical realizations (M), and the ensemble-averaged reflection R and transmission J of radiation are evaluated [24],

$$\langle R(t, z)\rangle = \frac{1}{M}\sum_{i=1}^{M}\int_{-1}^{0}|\mu|\psi_i(t, z, \mu)d\mu, \quad (2a)$$

$$\langle J(t, z)\rangle = \frac{1}{M}\sum_{i=1}^{M}\int_{0}^{1}\mu\psi_i(t, z, \mu)d\mu. \quad (2b)$$

Other physical observables of interest can readily be computed, e.g., the ensemble-averaged specific radiation intensity $\langle\psi(t, z, \mu)\rangle$, material energy density $\langle\phi(t, z)\rangle$, radiation density $\langle E(t, z)\rangle$, and radiation flux $\langle F(t, z)\rangle$. Here we are mainly concerned with the reflection from the incident edge $z = 0$, i.e., $\langle R(t, 0)\rangle$, and the transmission and material energy density at the outgoing edge $z = L$, i.e., $\langle J(t, L)\rangle$ and $\langle\phi(t, L)\rangle$. Occasionally, transmission and reflection probabilities will be involved, which are defined by the ratio of calculated values to incident radiation flux.

B. Numerical setups

We developed a parallel program [52] to generate the binary stochastic mixture and efficiently solve the time-dependent coupled transport equations (1). More details of numerical implementation can be found in Appendix A. In this work, we describe the binary stochastic mixture by using the variants of model parameters previously utilized in Ref. [38]: The mean chord lengths (λ_i, $i = 1$, 2) of materials 1 and 2 are $\lambda_1 = 5.6 \times 10^{-3}$ cm and $\lambda_2 = 5.0 \times 10^{-2}$ cm, which result in mixing probabilities of $p_1 = 10\%$ and $p_2 = 90\%$. The absorption opacities are $\sigma_{a,1} = 1000$ cm^{-1} and $\sigma_{a,2} = 5$ cm^{-1}, which differ by at least two orders of magnitude. The total length of the stochastic mixture is set equal to $L = 0.15$ cm. Here the parametrization results in a spatially homogeneous stochastic mixture statistically mixed by two distinct materials, e.g., a small amount of material 1 randomly distributed in material 2. The physical scenario is consistent with relevant experiments where a fraction of gold particles are admixed with a large amount of hydrocarbon foam [6,7],

TABLE I. Model parameters of the binary stochastic mixture and numerical parameters used in simulations.

Label	Parameters
Material 1	$\lambda_1 = 5.6 \times 10^{-3}$ cm, $p_1 = 0.1$, $\sigma_{a,1} = 10^3$ cm^{-1}
Material 2	$\lambda_2 = 5.0 \times 10^{-2}$ cm, $p_2 = 0.9$, $\sigma_{a,2} = 5$ cm^{-1}
Total length	$L = 0.15$ cm
Initial temperature	$T_0^m = 0.005$ keV
Radiation source	$T_0^r = 0.5$ keV
Angular direction	$N = 32$
Simulation time	$\tau = 500$ ps
Time step	$\Delta\tau = 1$ ps
Cell coefficient	$f = 0.2$
Convergent value	$\epsilon = 10^{-6}$
Realizations	$M = 10^5$

in the sense that the gold particles' absorption opacity is typically much higher than that of hydrocarbon foam by several orders of magnitude. In ICF simulations, it may describe a locally small volume in a large numerical area, which is occupied by materials randomly evolving in time between two distinct materials.

A source of radiation temperature at 0.5 keV presents at $z = 0$ and the materials' temperature is initially 0.005 keV. In other words, the present study deals with a cold stochastic mixture (i.e., a small amount of initial thermal energy) driven by a high-energy radiation source such as x rays. Angular variables are discretized into 32 directions, i.e., $N = 32$. A total simulation time of $\tau = 500$ ps is employed with a time step of $\Delta\tau = 1$ ps and the cell coefficient $f = 0.2$. The maximum cell size is 9.35×10^{-6} cm. The discretized cells are $N_1 \times N_2 \times N_3 = 500 \times 16\,044 \times 32$. The convergent value is sufficiently small, i.e., $\epsilon = 10^{-6}$, and a number of physical realizations $M = 10^5$ are sampled. For each mixture realization, identical parameters are applied, which are listed in Table I. It should be noted that, by using these parameters, energy conservation is automatically guaranteed (see Table III of the Supplemental Material [53]).

Moreover, we have explicitly performed a number of test calculations to validate the present numerical implementations, in order to increase the reliability of numerical results (see the first section in [53]). It is clear that our calculated results can quantitatively reproduce a variety of benchmark results reported in Refs. [29,38]. The consistency with the reported results establishes our confidence, allowing us to carry out the following study.

III. IMPACT OF RANDOM MEDIA

A. Mixing distribution

In the 1D slab model, the CLD is used to randomly sample the slab thickness of materials; thus various forms of CLDs result in different mixing distributions of random media. For the given mean chord length λ_i in Table I, we analyze the influence of the mixing distributions, based on five typical
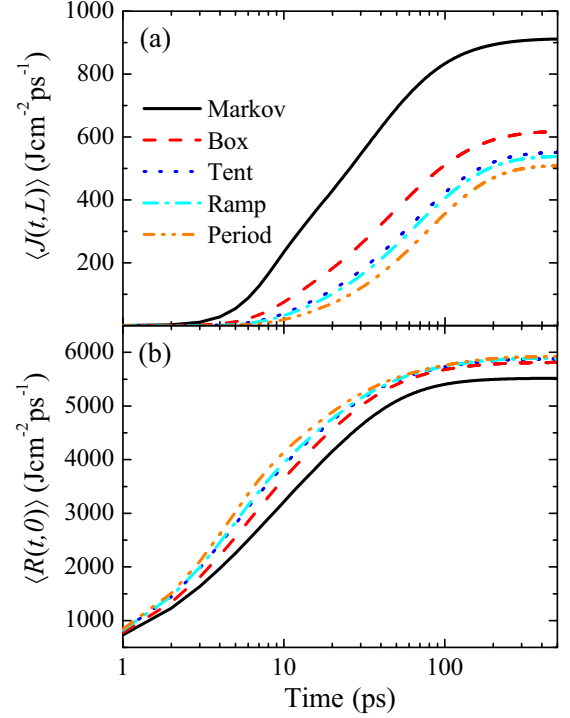

FIG. 2. (a) Ensemble-averaged transmission at the outgoing edge ($z = L$) as a function of time for five typical mixing distributions. (b) Same as (a) but for the reflection at the incident edge ($z = 0$). To better visualize the variance among the mixing distributions considered, the logarithmic scale is utilized for the horizontal axis.

CLDs [31,54] presented as

$$f_i(\xi) = \begin{cases} \frac{1}{\lambda_i}e^{-\xi/\lambda_i}, & \xi > 0 \quad \text{(Markov)} \\ \frac{1}{2\lambda_i}, & 0 < \xi \leqslant 2\lambda_i \quad \text{(box)} \\ \frac{\lambda_i + (\xi - \lambda_i)[2\Theta(\lambda_i - \xi) - 1]}{\lambda_i^2}, & 0 < \xi \leqslant 2\lambda_i \quad \text{(tent)} \\ \frac{8\xi}{9\lambda_i^2}, & 0 < \xi \leqslant 1.5\lambda_i \quad \text{(ramp)} \\ \delta(\xi - \lambda_i), & \xi > 0, \quad \text{(period)}. \end{cases}$$

(3)

In all cases, the chord length ξ is defined as positive. The Heaviside function Θ is introduced into the tent mixing to obtain a compact form. It should be noted that the CLDs considered are normalized to unity.

Figure 2 presents the ensemble-averaged transmission at the outgoing edge ($z = L$) and the reflection at the incident edge ($z = 0$). It is found that $\langle J(t, L) \rangle$ increases rapidly within 100 ps and stabilizes until 200 ps, which is true for all mixing distributions considered. It is not surprising that it imprints a similar tendency in $\langle \phi(t, L) \rangle$, and the Markov mixing distribution attains the strongest transmission and highest material energy density. Compared to the magnitude of the transmission, the reflection of radiation is more pronounced and it grows much faster during the nonequilibrium process, but its dependence on the mixing distribution is reversed. At steady-state times, the sum of the channels of the transmission and reflection amounts to the incident radiation flux due to energy
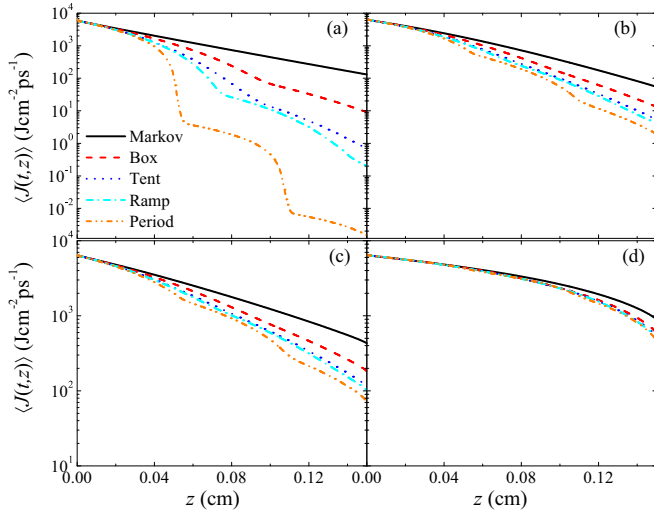
FIG. 3. Ensemble-averaged transmission as a function of position for calculations for the (a) nonparticipating and (b)–(d) participating random media, (a) independently of time and at (b) $t = 5$ ps, (c) $t = 20$ ps, and (d) $t = 200$ ps.

conservation (see [53] for more details) and the corresponding probabilities are 7.9%–14.2% and 85.8%–92.1%.

To facilitate the comparison among various mixing distributions, we simply define the enhanced factor as the ratio of the transmission from Markov mixing statistics to that from period mixing. For the nonparticipating random media, i.e., in the absence of material energy coupling, Fig. 3(a) shows that the enhanced factor of $\langle J(L) \rangle$ differs by about five orders of magnitude, which is entirely consistent with the observation in Ref. [31]. For the participating random media, the impact of mixing distributions depends sensitively on time [see Figs. 3(b)–3(d)]. As can be seen, the enhanced factor develops from one order of magnitude at 5 ps to ∼1.8 at steady-state times ($t = 500$ ps) in Fig. 2(a). The remarkable discrepancy is mostly due to the effect of material temperature. In the case of nonparticipating random media, the absorption and transmission of radiation are the only two channels of energy transport, which is dominated by the absorption of radiation, e.g., more than 97.9% energy has been absorbed; thereby the transmission is strongly sensitive to the distribution of the mixed materials, as observed in Fig. 3(a). However, when the material temperature is coupled to radiation, two additional energy transport channels emerge [53], i.e., radiation emission and reflection, and it is found that a large portion of incident radiation energy has been transported into the reflection channel [see Fig. 2(b)]. In other words, thermal radiation emission plays a key role in this case; thereby the transmission is closely related to the material temperature, which significantly suppresses the effect of the mixing distribution.

Furthermore, the radiation flux of various channels (i.e., absorption, emission, reflection, and transmission of radiation) is analyzed and we find that the reflection dominates over the other channels in all cases. At early times, radiation and material remain in the nonequilibrium state, resulting in more radiation absorbed than emitted, which is more notable for material 1 here. The situation is changed until 200 ps, at which time the absorption of radiation is nearly balanced by
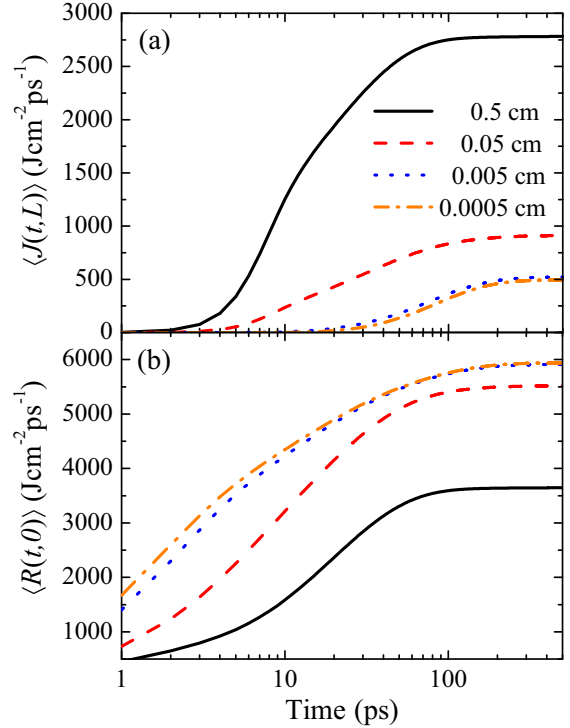

FIG. 4. Same as Fig. 2 but for (a) varying the mixture size using a Markov mixing distribution for $p_1 = 10\%$. Numbers indicated in the legend are λ_2 in units of cm.

the emission, and the transmission is less than 15%, regardless of mixing distributions. These results may suggest that thermal random media, as a source of radiation, can considerably weaken the impact of the stochastic mixtures' mixing distributions. To summarize, with the coupling of radiation to material, the variation of transmission at steady-state times is limited to less than a factor of 2 when varying the mixing distributions using the present parameters, which significantly deviates from that in purely absorbing cases.

B. Mixing size

Figures 4 and 5 show the impact of mixing size, when the size of the binary stochastic mixture is varied over a span of three orders of magnitude, i.e., from 0.5 to 0.0005 cm, within the Markov mixing distribution. By decreasing the mixing size, the ensemble-averaged transmission at the outgoing edge decreases for all times [see Fig. 4(a)]; specifically for steady-state times it is reduced by a factor of ∼5.63, i.e., the enhanced factor. This observation is also true for the ensemble-averaged material energy density. Conversely, the ensemble-averaged reflection from the incident edge is enhanced at steady-state times by a factor of ∼1.63 when decreasing the mixing size from 0.5 to 0.0005 cm. Clearly, the mixing size effect can be observed in both the transmission and reflection from very early times. Quantitatively, with the present parameters it seems that the impact of the mixing size is more impressive than that of the mixing distribution in Fig. 2. In this regard, it is somewhat in accordance with that in purely absorbing cases [31].
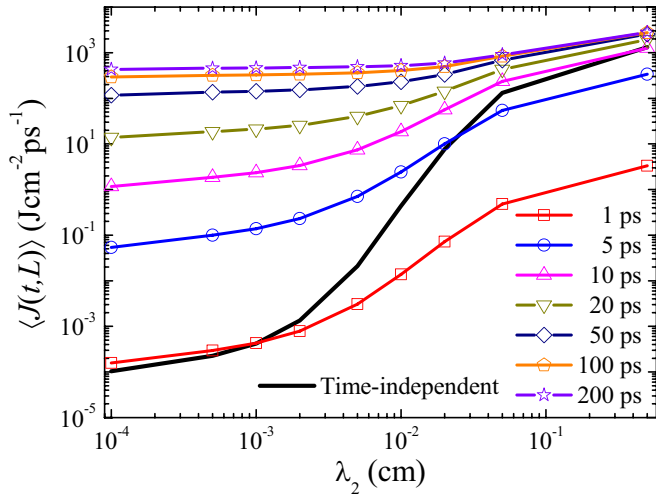
FIG. 5. Mixing size effect of binary Markovian mixtures on the ensemble-averaged transmission at the outgoing edge. The mixing size is varied from a fraction of a centimeter to 10 000 cm to 1 cm. Solid lines between symbols are plotted to guide the eyes. The results of nonparticipating random media (black solid curve) are shown for comparison. Note that logarithmic scales are used for both horizontal and vertical axes to facilitate the comparison.

Figure 5 depicts the size-dependent ensemble-averaged transmission at the outgoing edge for a sequence of times. Note that the results of nonparticipating random media are shown to facilitate the analysis. For the mixing size considered, the ensemble-averaged transmission through nonparticipating random media is varied among seven orders of magnitude, i.e., a very notable mixing size effect. In contrast, for participating random medium cases, the impact of the mixing size strongly depends on the time associated with the instantaneous material temperatures, resulting in the variation being limited, e.g., it attains nearly one, two, and three orders of magnitude at 100, 20, and 5 ps, respectively. At 500 ps, it is reduced to a factor of 5.63, which is much lower than that in nonparticipating random media (black solid curve). On the other hand, it is obvious that the steplike shape in the transmission in a range of 10^{-3}–10^{-1} cm has been softened with time evolving for participating random media, which is evidence that the mixing size effect can be restrained by thermal random media due to coupling of radiation to material.

Approaching the steady states, the reflection probabilities are about 56.7%–92.3% for the mixing sizes considered, which restricts the variation of the transmission of radiation with the mixing size less than one order of magnitude due to energy conservation [53]. In the case of nonparticipating random media, the physical scenario is changed as analyzed before, for which only absorption of radiation and transmission occur. In this situation, a large variation of transmission over the mixing size is not surprising, since pure absorption of radiation is sensitively dependent on the mixing size [31].

C. Mixing probability

Figure 6 presents results by varying the mixing probability of material 1 from 0.01 to 0.5, covering the range more than
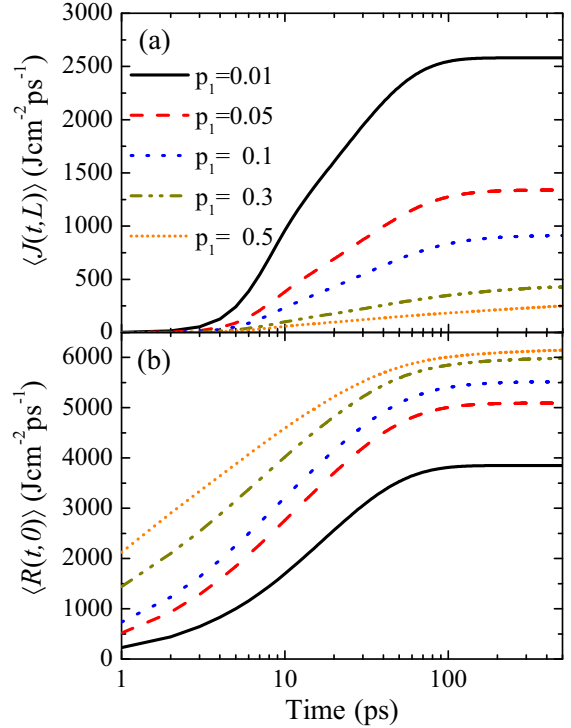

FIG. 6. Same as Fig. 2 but for (a) varying the mixture probability of material 1.

one order of magnitude. As can be seen in Fig. 6(a), the transmission decreases monotonically while increasing the mixing probability, and at steady state the case of $p_1 = 0.01$ leads to the strongest transmission, larger than that of $p_1 = 0.1$ and 0.5 by factors of 2.83 and 10.36, respectively. From an analysis of the radiation flux of various channels, we find that absorption of radiation is totally dominated by the amount of constituent material that has higher opacity; for instance, at steady-state times the absorption for a mixing probability of 50% of material 1 is larger than that for 1% by a factor of ~30, and the contribution of material 1 to the respective absorption of radiation accounts for 99.5% and 66.7%. With the coupling of radiation to material, the absorption and emission of radiation undergo a nonequilibrium to equilibrium process, and the more material 1 is mixed, the more the emission of radiation is enhanced, which results in stronger reflections. This analysis is consistent with the observation of the reflection in Fig. 6(b). Compared to the influence of the mixing distribution and size analyzed in previous sections, it is found that the stochastic radiation transport is the most sensitive to the mixing probability, suggesting that the physical scenario of radiation transport through participating random media is much different from that in nonparticipating stochastic mixtures [24,26–29,31].

Figure 7 compares the ensemble-averaged transmissions from several typical times with that in nonparticipating random medium calculations. Regardless of time, the mixing probabilities in the considered range always result in the transmission varying within an order of magnitude, indicating that the relation of the transmission to the mixing probability is rather stable against time, which is different from the
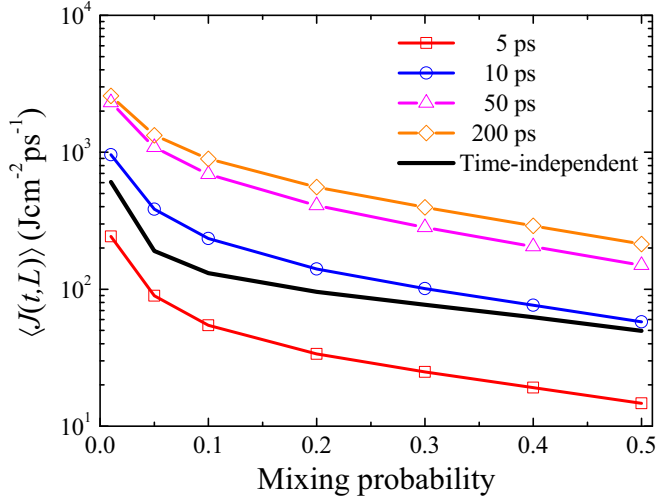
FIG. 7. Mixing-probability-dependent ensemble-averaged transmission at the outgoing edge for binary Markovian mixtures. The mixing probability is tuned over one order of magnitude, i.e., from 0.01 to 0.5. Solid lines between symbols are plotted to guide the eyes. The results of nonparticipating random media (black solid curve) are shown to facilitate the comparison.

observation in Figs. 3 and 5. In addition, quantitative deviations appear in the calculations of nonpartic-

ipating random media, e.g., the transmissions for $p_1 = 0.01$ and 0.5 are lower than the steady-state values (i.e, $t = 500$ ps) by factors of 4.26 and 4.32, respectively. However, the transmission has a similar shape, agreeing particularly well with those values at 10 ps, which is again distinct from similar comparisons when varying the mixing distribution and size.

IV. MODELING THE ENSEMBLE-AVERAGED TRANSMISSION OF RADIATION

A. Role of material temperature revisited

In the preceding section, we have seen how the impact of a random medium on the stochastic radiation transport can be substantially changed by material temperatures. Typically, it is known that the material itself is a temperature-dependent source of radiation [49]; however, in a binary stochastic mixture, an in-depth understanding of the contribution of material temperature to the transmission of radiation has not yet been explicitly attained. For this purpose, we built a steady-state stochastic transport model for a specified direction μ, which allows us to include material temperatures as a source of emission. Fortunately, with multiple algebraic manipulations (see Appendix B for more details), the ensemble-averaged specific radiation intensity for the direction μ can be analytically solved as

$$\underbrace{\langle \psi_\mu(z) \rangle}_{\text{I}} \approx \underbrace{\psi_0[we^{\varepsilon_+ z} + (1-w)e^{\varepsilon_- z}]}_{\text{II}} + \underbrace{\langle B(z) \rangle \frac{1 + \langle \sigma_a(z)B(z) \rangle / \sigma_{a,1}\sigma_{a,2}\lambda_c \langle B(z) \rangle}{1 + \langle \sigma_a(z) \rangle / \sigma_{a,1}\sigma_{a,2}\lambda_c} \{1 - [we^{\varepsilon_+ z} + (1-w)e^{\varepsilon_- z}]\}}_{\text{III}}, \quad (4)$$

where ψ_0 specifies the incident radiation intensity at $z = 0$, w and $\varepsilon_\pm$ are fractional weights and exponential factors of purely absorbing cases, respectively, which can be analytically computed by stochastic the mixtures' parameters [21,22], and $B(z)$ is the Planck function determined by the local material temperature $T(z)$. Detailed explanations of the derived parameters can be found in Appendix B. Integrating over the forward directions, the ensemble-averaged transmission is given as

$$\langle J(z) \rangle = \int_0^1 \mu \langle \psi_\mu(z) \rangle d\mu. \quad (5)$$

In the steady-state stochastic transport model, the ensemble-averaged intensity (term I) can be simply factorized into two terms: Term II describes radiation transport through nonparticipating random media, i.e., independently of temperature, and term III considers thermal emissions weighted by the probability of unabsorbed photons. With this model, the ensemble-averaged transmission through participating random media is simply that through nonparticipating random media augmented by a term related to material temperature, which is plausible. For a given direction μ, term II is independent of temperature, while term III implicitly depends on the material temperature which is involved in $B(z)$.

Although the derivation of Eq. (4) neglects the time derivative, it still makes sense to see to what extent the analytical

and simulated results can be compared, for photon transport in stochastic mixtures. To obtain the analytical transmission, the ensemble-averaged material temperature and its statistical correlation are calculated for all cells at each time step in simulations based on the parameters in Table I. We first show the comparison of normalized transmissions as functions of time and space in Fig. 8. Generally, the analytical results agree satisfactorily with simulated data, e.g., a time-varying profile of the ensemble-averaged transmission is well reproduced,
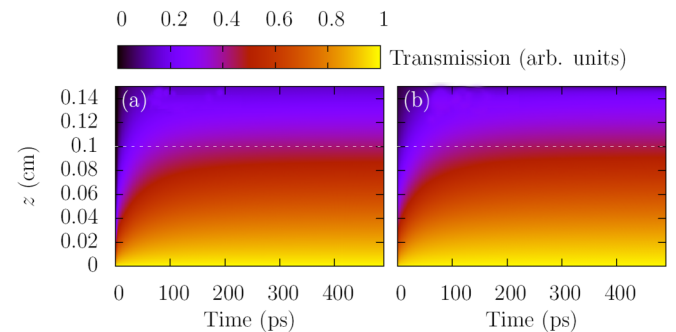

FIG. 8. Ensemble-averaged transmission: (a) numeric results calculated by solving Eqs. (1) over 10^5 physical realizations and (b) analytic results (term I) based on Eq. (4). The color bars are normalized. Dashed lines roughly label the steady states.
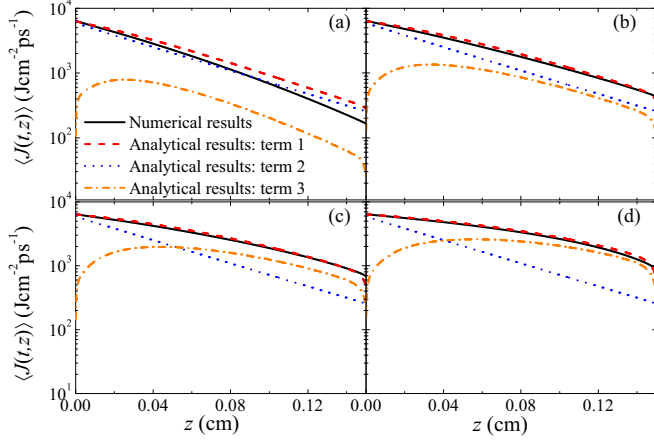
FIG. 9. Comparison of spatial-dependent ensemble-averaged transmission between numerical and analytical results for a sequence of times: (a) 8 ps, (b) 20 ps, (c) 50 ps, and (d) 200 ps.

especially both the steady-state magnitude (labeled by dashed lines) and the relaxation time.

Figure 9 explicitly evaluates the steady-state stochastic transport model by comparing it to numerical results at four typical times. At 8 ps, the transmission is dominated by the radiation absorption through nonparticipating random media (term 2) everywhere, which is larger than thermal emission (term 3) by nearly an order of magnitude. At 20 ps, the radiation absorption only prevails at short distances, i.e., $z \leqslant 0.06$ cm, beyond which the contribution of thermal emission is comparable. At 50 and 200 ps, thermal emission grows into the leading agent at intermediate to large distances (e.g., $z \geqslant 0.04$ cm). Interestingly, the intersection of the pure absorbing and thermal emission curves at final times happens to emerge in the vicinity of the photons' mean free path (MFP) through a nonparticipating random medium [22,31,54], i.e., $l_p = 0.042$ cm. In all cases, analytic results (dashed curves) predict the numerical ones (solid curves) very well.

We further show the contributions of the radiation absorption and thermal emission to ensemble-averaged transmission in Fig. 10. It is obvious that the mechanism of transmission of radiation is distance dependent, which is determined by the thermal emission. Pure radiation absorption is dominated in the regime of $z \leqslant 0.04$ cm and thermal emission is fairly important in the other regime. It is apparent that the transition
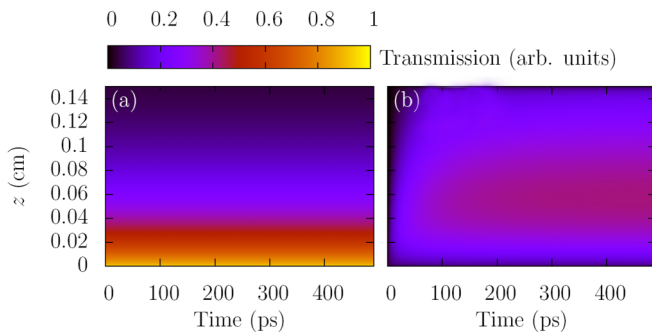

FIG. 10. Separate contributions of ensemble-averaged transmission in Eq. (4): (a) term II and (b) term III.

from nonequilibrium to the equilibrium state in the transmission is mainly dictated by thermal emissions [see Fig. 10(b)]. Note that we have also evaluated the applicability of the steady-state stochastic transport model in the cases displayed in Sec. III, which is in accordance with the observation here. A systematic analysis reveals that the regime of two different contributions is somehow correlated to the MFP of photons in nonparticipating random media. All in all, the analytic model is able to capture the essentials of the nonequilibrium radiation transport process, and it makes sense provided that the material temperature is well measured.

B. Mechanism of the impact of random media

Based on the steady-state stochastic transport model above, the ensemble-averaged transmission at the outgoing edge ($z = L$) can be largely affected by the material temperature, which competes with pure radiation absorption in a certain region; therefore, the length (l_p) distinguishing these two physical processes is extremely crucial. It can be speculated that if $l_p < L$, the material temperature plays a key role in the determination of the transmission, and a pronounced dependence of the transmission on the random media may result from the variation of the value of l_p when varying the properties of random media. In contrast, if $l_p \gtrsim L$, it is dominated by pure absorption of radiation, which does not depend on the microscopic properties of random media (e.g., mixing distribution and size) at short distances [27,31] (see Fig. 3).

Within the above propositions, the findings in Sec. III, i.e., the impact of the mixing probability on the transmission is the most pronounced, followed by the mixing size, and the mixing distribution has a very limited influence, can be understood as follows. By varying the mixing distributions considered, l_p is varied from 0.04 cm (Markov) to 0.02 cm (period), which are always much smaller than the total width of a random medium $L = 0.15$ cm. In this case, the transmission is dominated by material temperatures, which do not have significant deviations between Markov and period mixing distributions, since l_p is quite close in both cases. This can explain the weak dependence on the mixing statistics in Fig. 2(a). By decreasing the mixing sizes used, l_p is tuned from 0.13 cm to 0.01 cm, which ranges from the region comparable to L to that much lower than L. In this situation, the transmission of large mixing sizes (high l_p) is dominated by pure radiation absorption, while for small mixing sizes (low l_p) the material temperature effect is remarkable. Altogether these result in a moderate dependence on the mixing size in Fig. 4(a). When increasing the mixing probability, l_p is changed from 0.09 cm to 0.02 cm, which are smaller than L. In all cases, material temperatures are the essential factor. As the redistribution of thermal radiations decays exponentially with increasing distance, it is not surprising that the mixing probability acquires the most noticeable effect on the transmission.

To further verify our explanations, we have performed systematic calculations for a variety of L using the parameters in Table I. For clarity, we only compare the enhanced factor when tuning the properties of random media, i.e., the ratio of the highest ensemble-averaged transmission to the lowest value at 500 ps. Simulated results are shown in Fig. 11(a). It can be seen that for $L \leqslant 0.01$ cm, the enhanced factor in
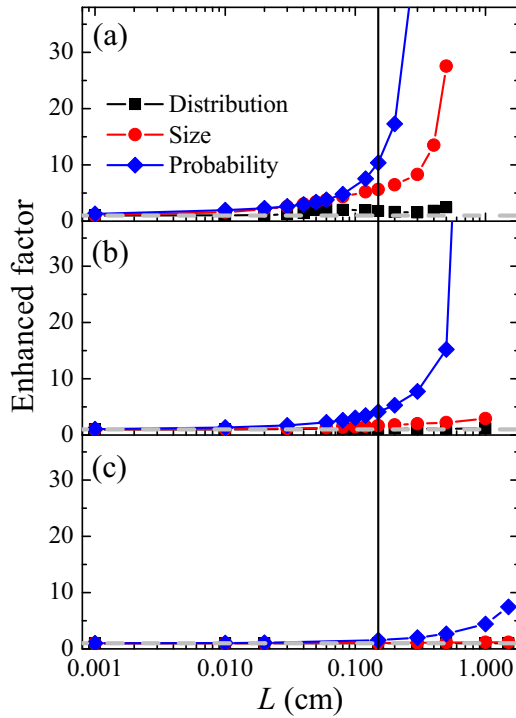
FIG. 11. Enhanced factor due to the variation of the properties of random media as a function of L for (a) $\sigma_{a,i}$, (b) $\sigma_{a,i}/10$, and (c) $\sigma_{a,i}/100$. (a) The opacities are $\sigma_{a,1} = 10^3$ cm^{-1} and $\sigma_{a,2} = 5$ cm^{-1}. (b) The opacities of materials 1 and 2 are lower than those in (a) by one order of magnitude. (c) Same as (b) but lower than those in (a) by two orders of magnitude. Vertical lines label the position of $L = 0.15$ cm used in Table I. Symbols are connected by solid lines to guide the eyes and the gray dashed lines indicate no enhancements.

all cases is close to 1, i.e., random media can hardly affect the stochastic radiation transport in this regime. Note that L in this range is small enough compared to the minimal l_p (=0.02 cm). With increasing L, the enhanced factor of the mixing size and probability is rapidly growing, while for the mixing distribution it stays near the regime of no enhancements (gray dashed lines). Basically, for a given L the enhanced factor is invariably the highest for the mixing probability, which supports the findings in Sec. III. Obviously, the observation in Fig. 11(a) is consistent with the above propositions.

According to Refs. [22,31,54], l_p is associated with the constituent materials' opacities, which may impact the sensitivity of the transmission to the properties of random media relative to L. To illustrate it, we have decreased the opacities used in Fig. 11(a) by one and two orders of magnitude, respectively, and the results are shown in Figs. 11(b) and 11(c). Compared to Fig. 11(a), the development of the enhanced factor is visibly shifted to larger L, which is because l_p is considerably increased by decreasing the opacities of binary stochastic mixtures. For instance, for the mixing probability in Fig. 11(b), l_p ranges between 0.69 cm ($p_1 = 0.01$) and 0.04 cm ($p_1 = 0.5$), and for that in Fig. 11(c), l_p is varied between 6.76 and 0.22 cm. For these two cases, if the total width of a random medium identical to that widely used in Sec. III, i.e., $L = 0.15$ cm, it goes from $l_p > L$ to $l_p < L$ in Fig. 11(b) by decreasing p_1, which results in a suppressed mixing prob-

ability effect, while in Fig. 11(c) it satisfies $l_p \gg L$ for any p_1 considered, leading to a marginal effect of the mixing probability. Quantitatively, by varying the mixing distribution, size, and probability in the range studied, the enhanced factor is ordered as 1.79, 5.63, and 10.36 in Fig. 11(a), 1.14, 1.65, and 4.14 in Fig. 11(b), and 1.00, 1.04, and 1.52 Fig. 11(c).

Overall, the results in Fig. 11 confirm the fact that the impact of random media on the stochastic radiation transport is mainly determined by the relationship between l_p and L, and only the width of the random medium sufficiently larger than l_p can yield a remarkable dependence of radiation transport on the random media.

V. SELF-CONSISTENT ANALYSIS OF REPORTED MULTIDIMENSIONAL RESULTS

As it was disputable in previous multidimensional simulations [41,44,48] whether or not the properties of random media can considerably affect the radiation transport (see the Introduction), here we attempt to address this issue by combining the aforementioned simple relationship and 1D slab simulations. Although it was argued that 1D slab results are fundamentally different from 2D and 3D solutions [41], basic features of the dependence of transmission on the random media's properties in 1D cases may be similar to those in multidimensions.

In Ref. [41] Olson performed 2D simulations of stochastic radiative transfer in participating random media and claimed that "[the] results do not strongly depend on the details of the stochastic medium …. Very different disk/sphere sizes give similar results as long as the fraction of the area/volume occupied is the same." To understand those results, we have performed 1D calculations using identical parameters (see Table 1 in Ref. [41]). Similarly, the enhanced factor of radiation flux is defined to quantify the influence of random media. We find that the present enhanced factor for $L = 1.0$ (the width used by Olson [41]) nearly approaches 1.0 by varying the properties of random media, which is fully understandable in the following. For the parameters investigated, l_p is restricted to 1.0–2.03, which invariably fulfills the relation of $l_p \geqslant L = 1.0$. According to the mechanism of the impact of random media proposed in Sec. IV B and the results in Fig. 11, it is not surprising that the radiation flux is not sensitively dependent on the properties of the random medium. At this point, our 1D results are entirely consistent with the observation in Ref. [41]. In addition, a similar analysis in Ref. [44] based on 1D simulations revealed that the mixing distribution can indeed hardly affect the radiation flux.

In Ref. [48] Brantley and Martos reported results for nonparticipating random media and stated that "[their] benchmark results exhibit a significant dependence of the ensemble-averaged fiducial tallies on both sphere mean chord length and sphere volume fraction … [and] a weaker dependence on the distribution describing the sphere radii." To interpret this, we have again made 1D calculations based on the parameters used in the original work [48], which are summarized in Fig. 12. Note that Brantley and Martos utilized $L = 10.0$ in their study. We find that the calculated enhanced factors for mixing distributions, sizes, and probabilities are 10.42, 2.55, and 153 940, respectively, which generally agree with the 3D
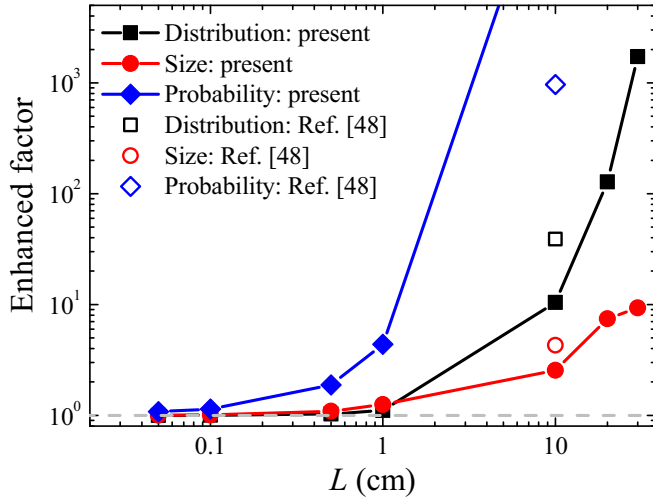
FIG. 12. Enhanced factor as a function of L using parameters identical to those in [48]. Three-dimensional results (open symbols) in Ref. [48] for $L = 10$ cm are shown for comparison. The gray dashed line highlights no impact of random media on the radiation flux.

results reported by Brantley and Martos [48]. The discrepancy might be attributed to the effect of dimensionality, which requires more calculations. For the parameters considered, l_p ranges from 0.44 to 3.41, which satisfies the condition $l_p \ll L = 10.0$. Within the proposition in Sec. IV B, the pronounced dependence on the random medium's properties can be understood reasonably well.

Based on our 1D slab results, we find that the multidimensional results of Olson [41] and Brantley and Martos [48] are essentially consistent in terms of the relationship between l_p and L. In the case of Olson [41], the enhanced factor is limited to less than a factor of 2 even if the L is increased to large values, e.g., $L = 7.0$, mostly probably due to a narrow variation of l_p. It should be noted that the ensemble-averaged opacity is always set equal to 1.0 when varying the properties of a random medium in Ref. [41], while in the case of Brantley and Martos [48] one may see a very weak impact of a random medium if the L is dropped to small values, e.g., $L = 0.1$, which is much smaller than the minimal l_p (see Fig. 12). In addition, the notable impact of the random medium observed by Brantley and Martos [48] can also be suppressed to some degree when the coupling of radiation to material is included, as widely discussed in Sec. III.

VI. CONCLUSION

By using a random sampling of mixtures combined with a deterministic solution of the time-dependent radiation transport equation coupled to a material temperature equation, we have systematically studied stochastic radiative transfer in binary random media in the planar geometry. First, we have systematically shown and analyzed the impact of the mixing distribution, size, and probability of binary stochastic mixtures on the radiation transport. By comparing these results with those in purely absorbing cases, we found that only the influence of mixing probability is similar to that in purely absorbing cases, while the impact of the mixing distribution and

size is significantly suppressed by introducing the radiation coupled to the material temperature, which is understood by the analysis of energy transport channels.

Second, the role of material temperature in stochastic radiative transfer in binary random media was analyzed by deriving a steady-state stochastic transport model. It was found that analytical ensemble-averaged transmissions agree very well with numerical simulations. The mechanism of transmission of radiation is distance dependent, which is closely related to the mean free path of photons l_p. For $z \lesssim l_p$, pure absorption is dominant, and beyond this regime thermal radiation emission is gradually growing into the leading factor with increasing time. Only with inclusion of material temperature coupling can it well describe the transition from nonequilibrium to the equilibrium state.

A remarkable finding in this work is that the mechanism of the impact of random media on the stochastic radiation transport is mainly determined by the relationship between l_p and L. For $l_p < L$, a pronounced dependence of the transmission on the random media results from a variation of the value of l_p by varying the properties of random media, while for $l_p \gtrsim L$, pure absorption of radiation plays a role, resulting in nearly identical radiation flux for various mixing distributions and sizes, since at short distances it is insensitive to the microscopic properties of random media. This proposition was further confirmed by more calculations with the constituent materials' opacities reduced by one and two orders of magnitude.

Most importantly, combining this simple relationship and 1D simulations, we have resolved the disputable issue of the impact of random medium in previous multidimensional simulations. It was found that the existing multidimensional results of Olson [41] and Brantley and Martos [48] are basically consistent and the observed weak or remarkable impact of random media is mainly due to a distinctly different relationship between l_p and L. By tuning the L, one can enhance or suppress the impact of random media on the stochastic radiation transport, provided l_p can be varied in a relatively wide range for the parameters studied. Our results may also find applications in relevant experiments to test models of stochastic radiative transfer, in which the length of the tube containing the stochastic mixture is a crucial parameter to determine the impact of random medium.

Additionally, there are some limitations of present work. First of all, temperature-dependent opacity is neglected, but could readily be implemented. In this situation, the mean free path will be updated at each time step, resulting in its relationship with the width of the random medium complicated. Second, our study lacks the multigroup effect, which may affect the magnitude of radiation flux. Finally, a direct comparison of radiation flux with configurations in more than one dimension is absent.

The simulation code and data of relevance in this study are available from the corresponding authors upon reasonable request.

APPENDIX A: NUMERICAL IMPLEMENTATION

In practical implementation, ψ is discretized into numerical cells as $\psi(t_n, z_k, \mu_m)$, in which t_n, z_k, and μ_m denote discrete variables with $n = 1, 2, \ldots, N_1$; $k = 1/2, 3/2, \ldots, (2N_2 - 1)/2$; and $m = 1, 2, \ldots, N_3$, where N_1, N_2, and N_3 correspond to the total number of cells discretized for each variable. Meanwhile, ϕ is numerically represented by $\phi(t_n, z_j)$ with $j = 1, 2, \ldots, N_2 - 1$. Typically, temporal and spatial discretizations are realized by a staggered cell with ψ at the faces of the cells and ϕ at the centers of the cells, respectively. Regarding the numerical algorithms, we employed the diamond difference method for spatial discretization of the differential operator [55], the implicit time discretization for the radiation intensity and material energy density derivatives, and the discrete ordinate method (S_N) for the angular discretization [55]. At each time step in simulations, we used the source iteration approach to update the ψ and ϕ simultaneously until the maximal relative difference of the radiation intensity and material energy density between the successive iteration steps was equivalent to or lower than the convergent criterion ϵ. Test calculations show that the present discretization strategy can quantitatively reproduce the benchmark results reported in previous stochastic radiative transfer studies [24,27,29,38] (see the first section in [53]).

The assumed nonrandom initial and boundary conditions are given as follows. It is assumed that initially the stochastic mixture is cold with a homogeneous temperature of T_0^m, and thus for any cell z_k and any direction μ_m the initial conditions are

$$\phi(t = 0, z_k) = a\left(T_0^m\right)^4, \quad \psi(t = 0, z_k, \mu_m) = \sigma_{SB}\left(T_0^m\right)^4, \tag{A1}$$

where σ_{SB} is the Stefan-Boltzmann constant (equal to 1.03×10^{-7} J cm^{-2} eV^{-4} ps^{-1}). In the presence of a radiation source at $z = 0$, i.e., an initial radiation temperature of T_0^r, the photons impinge perpendicularly upon the left surface of the stochastic mixture and propagate forward ($\mu_m > 0$), while at the other edge $z = L$ the radiation source is absent, which means that the source of the photons' backward propagation ($\mu_m < 0$) is vanishing; accordingly, the boundary conditions are set equal to

$$\psi(t, z = 0, \mu_m > 0) = 2\sigma_{SB}\left(T_0^r\right)^4, \tag{A2a}$$

$$\psi(t, z = L, \mu_m < 0) = 0. \tag{A2b}$$

In addition, the convergence of numerical parameters has been evaluated. Taking the transmission at the outgoing edge at steady-state times as an example, it is found that upon varying the total number of realizations M between 10^5 and 10^7, the relative error is smaller than 0.3%; varying the quadrature ordinates N between 16 and 128, it is lower than 0.08%; varying the time step $\Delta\tau$ between 0.001 and 1 ps, it is lower than 0.4%; varying the random number used in the sam-

pling of the stochastic mixture, the relative error is limited to $\sim$0.3%. It should be noted that the cell size Δz_k is dependent on the N and $\Delta\tau$ in our calculations, so its impact on the results has already been included when modifying relevant parameters. As a result, the parameters in Table I are adequate to supply the present analysis, which can ensure a good balance between the computational expense and numerical accuracy.

Actually, the numerical approach we used here proves more than adequate to provide relatively accurate results. Readers interested in the development of a different sampling method of generating the stochastic mixture and/or other numerical schemes to solve the coupled transport equations are referred to Refs. [56–59].

APPENDIX B: STEADY-STATE STOCHASTIC TRANSPORT MODEL

For the process of radiation absorption and emission in the time-independent condition, the transport of radiation for a specified direction μ in a 1D planar binary random mixture is described by the equation [24]

$$\mu\frac{\partial}{\partial z}\psi(z, \mu) + \sigma_a(z)\psi(z, \mu) = S(z), \tag{B1}$$

where $\sigma_a(z)$ and $S(z)$ are the absorption opacity and emission source, respectively; both are material dependent, i.e., $\sigma_a(z) = \sigma_{a,1}$ and $S(z) = \sigma_{a,1}B(T_1)$ if material 1 appears at z and otherwise $\sigma_a(z) = \sigma_{a,2}$ and $S(z) = \sigma_{a,2}B(T_2)$, where the radiation emission follows Kirchoff's law. Material 1 (2) is assumed to have a temperature of T_1 (T_2), which may depend on the spatial position.

A direction-independent equation can be established by dividing μ in Eq. (B1), giving

$$\frac{\partial}{\partial z}\psi(z, \mu) + \sigma_a'(z)\psi(z, \mu) = S'(z),$$

$$\sigma_a'(z) = \frac{\sigma_a(z)}{\mu}, \quad S'(z) = \frac{S(z)}{\mu} = \sigma_a'(z)B(T). \tag{B2}$$

For simplicity, we will ignore the symbols with superscripts and μ in ψ; thereby the stochastic radiation transport equation can be formally expressed as

$$\frac{\partial}{\partial z}\psi(z) + \sigma_a(z)\psi(z) = S(z). \tag{B3}$$

Within the Markov mixing distribution, it has been shown that the stochastic equation (B3) can be converted to a set of two coupled deterministic equations involving the ensemble-averaged radiation intensity $\langle\psi\rangle$ [54],

$$\frac{d\langle\psi\rangle}{dz} + \langle\sigma_a\rangle\langle\psi\rangle + \gamma\chi = \langle S\rangle, \tag{B4a}$$

$$\frac{d\chi}{dz} + \gamma\langle\psi\rangle + \hat{\sigma}_a\chi = T, \tag{B4b}$$

where χ is the other unknown variable which is related to the material-dependent radiation intensity ψ_i ($i = 1, 2$), i.e.,

$\chi = \sqrt{p_1 p_2}(\psi_1 - \psi_2)$, and the other parameters are defined by

$$\langle S \rangle = p_1 S_1 + p_2 S_2, \quad T = \sqrt{p_1 p_2}(S_1 - S_2),$$
$$\langle \sigma_a \rangle = p_1 \sigma_{a,1} + p_2 \sigma_{a,2}, \quad \gamma = \sqrt{p_1 p_2}(\sigma_{a,1} - \sigma_{a,2}),$$
$$\hat{\sigma}_a = p_2 \sigma_{a,1} + p_1 \sigma_{a,2} + \frac{1}{\lambda_c}. \tag{B5}$$

It is clear that Eq. (B4) is analytically tractable, which can be decomposed into two parts as

$$\langle \psi(z) \rangle = \langle \psi(z) \rangle_{\text{homo}} + \langle \psi(z) \rangle_{\text{nonhomo}}, \tag{B6}$$

where $\langle \psi(z) \rangle_{\text{homo}}$ is the homogeneous solution in the purely absorbing case, i.e., neglecting $\langle S \rangle$ and T, and $\langle \psi(z) \rangle_{\text{nonhomo}}$ is the solution of equations that discard the differential operators. With multiple mathematical manipulations, the solution of the homogeneous equations [21,22] is

$$\langle \psi(z) \rangle_{\text{homo}} = A[w \exp(\varepsilon_+ z) + (1 - w) \exp(\varepsilon_- z)], \tag{B7}$$

with the parameters defined as

$$\varepsilon_{\pm} = \frac{-(\langle \sigma_a \rangle + \hat{\sigma}_a) \pm \sqrt{\Delta}}{2}, \tag{B8a}$$

$$w = \frac{1}{2} - \frac{\langle \sigma_a \rangle - \hat{\sigma}_a}{2\sqrt{\Delta}}, \tag{B8b}$$

$$\Delta = (\langle \sigma_a \rangle - \hat{\sigma}_a)^2 + 4\gamma^2. \tag{B8c}$$

It should be mentioned that the exponential factors $\varepsilon_{\pm}$ are always negative and the weight w is a fraction of unity. Here A is an unknown coefficient to be determined in the following.

The solution of the nonhomogeneous equation can be readily written as

$$\langle \psi(z) \rangle_{\text{nonhomo}} = \frac{1}{|M|}[\hat{\sigma}_a \langle S(z) \rangle - \gamma T(z)], \tag{B9}$$

with M in the matrix form

$$M = \begin{pmatrix} -\langle \sigma_a \rangle & -\gamma \\ -\gamma & -\hat{\sigma}_a \end{pmatrix}. \tag{B10}$$

To determine the coefficient A, we utilize the initial condition of the problem. Suppose the incident radiation intensity is ψ_0 (nonstochastic) at $z = 0$; combined with Eqs. (B6)–(B10), we have

$$\langle \psi(0) \rangle = \psi_0 = A + \frac{1}{|M|}[\hat{\sigma}_a \langle S(0) \rangle - \gamma T(0)]. \tag{B11}$$

Substituting Eqs. (B7), (B9), and (B11) into Eq. (B6) and making proper arrangements for similar terms, we arrive

at

$$\langle \psi(z) \rangle \approx \psi_0[w \exp(\varepsilon_+ z) + (1 - w) \exp(\varepsilon_- z)]$$
$$+ \frac{1}{|M|}[\hat{\sigma}_a \langle S(z) \rangle - \gamma T(z)]$$
$$\times \{1 - [w \exp(\varepsilon_+ z) + (1 - w) \exp(\varepsilon_- z)]\}. \tag{B12}$$

The approximation is made by assuming that related source terms $\langle S \rangle$ and T are weakly dependent on spatial coordinates, which may be invalid for stochastic mixtures with large L. In a dynamical radiation-emission process, materials at finite temperatures at arbitrary positions can be regarded as initial point sources of thermal radiation with respect to the transmission at the exiting edge. It remains to work out the expressions of $|M|$ and $\hat{\sigma}_a \langle S \rangle - \gamma T$,

$$|M| = \langle \sigma_a \rangle \hat{\sigma}_a - \gamma^2$$
$$= \langle \sigma_a \rangle \left(\sigma_{a,1} + \sigma_{a,2} - \langle \sigma_a \rangle + \frac{1}{\lambda_c} \right) - p_1 p_2 (\sigma_{a,1} - \sigma_{a,2})^2$$
$$= p_1^2 \sigma_{a,1}^2 + 2 p_1 p_2 \sigma_{a,1} \sigma_{a,2} + p_2^2 \sigma_{a,2}^2$$
$$+ \sigma_{a,1} \sigma_{a,2} - \langle \sigma_a \rangle^2 + \langle \sigma_a \rangle \frac{1}{\lambda_c}$$
$$= \sigma_{a,1} \sigma_{a,2} + \langle \sigma_a \rangle \frac{1}{\lambda_c} \tag{B13}$$

and

$$\hat{\sigma}_a \langle S \rangle - \gamma T$$
$$= \left(p_1 \sigma_{a,2} + p_2 \sigma_{a,1} + \frac{1}{\lambda_c} \right)(p_1 \sigma_{a,1} B_1 + p_2 \sigma_{a,2} B_2)$$
$$- p_1 p_2 (\sigma_{a,1} - \sigma_{a,2})(\sigma_{a,1} B_1 - \sigma_{a,2} B_2)$$
$$= \sigma_{a,1} \sigma_{a,2} \langle B \rangle + \langle \sigma_a B \rangle \frac{1}{\lambda_c}, \tag{B14}$$

which can be further inserted into Eq. (B12) to obtain

$$\langle \psi(z) \rangle \approx \psi_0[w \exp(\varepsilon_+ z) + (1 - w) \exp(\varepsilon_- z)]$$
$$+ \langle B(z) \rangle \frac{1 + \langle \sigma_a(z) B(z) \rangle / \sigma_{a,1} \sigma_{a,2} \lambda_c \langle B(z) \rangle}{1 + \langle \sigma_a(z) \rangle / \sigma_{a,1} \sigma_{a,2} \lambda_c}$$
$$\times \{1 - [w \exp(\varepsilon_+ z) + (1 - w) \exp(\varepsilon_- z)]\}, \tag{B15}$$

which is the formula presented in Eq. (4). To evaluate the ensemble-averaged transmission in the forward directions ($\mu > 0$), one has to take into account the direction modified absorption opacity in Eq. (B2) and numerically integrate the direction of the weighted ensemble-averaged intensity over all forward directions [see Eq. (5)].

[1] S. Torquato, *Random Heterogeneous Materials: Microstructure and Macroscopic Properties* (Springer Science + Business Media, New York, 2013), Vol. 16.

[2] P. Boissé, Radiative transfer inside clumpy media-the penetration of UV photons inside molecular clouds, Astron. Astrophys. **228**, 483 (1990).

[3] A. Belleni-Morante and G. Saccomandi, Time dependent photon transport in a three dimensional interstellar cloud with stochastic clumps, Astrophys. Space Sci. **234**, 85 (1995).

[4] C. Cecchi-Pestellini and L. Barletti, Radiative transfer in a stochastic universe: I. Observation-related statistics, New Astron. **6**, 151 (2001).

[5] G. C. Pomraning, Radiative transfer in Rayleigh–Taylor unstable ICF pellets, Laser Part. Beams **8**, 741 (1990).

[6] P. A. Rosen, J. M. Foster, M. J. Taylor, P. A. Keiter, C. C. Smith, J. R. Finke, M. Gunderson, and T. S. Perry, Experiments to study radiation transport in clumpy media, Astrophys. Space Sci. **307**, 213 (2007).

[7] P. Keiter, M. Gunderson, J. Foster, P. Rosen, A. Comley, M. Taylor, and T. Perry, Radiation transport in inhomogeneous media, Phys. Plasmas **15**, 056901 (2008).

[8] R. Sanchez and G. C. Pomraning, A statistical analysis of the double heterogeneity problem, Ann. Nucl. Energy **18**, 371 (1991).

[9] R. Vasques and E. W. Larsen, Non-classical particle transport with angular-dependent path-length distributions. II: Application to pebble bed reactor cores, Ann. Nucl. Energy **70**, 301 (2014).

[10] C. Liang, A. T. Pavlou, and W. Ji, Effects of fuel particle size distributions on neutron transport in stochastic media, Ann. Nucl. Energy **68**, 146 (2014).

[11] C. Larmier, A. Zoia, F. Malvagi, E. Dumonteil, and A. Mazzolo, Neutron multiplication in random media: Reactivity and kinetics parameters, Ann. Nucl. Energy **111**, 391 (2018).

[12] F. Malvagi, R. Byrne, G. C. Pomraning, and R. Somerville, Stochastic radiative transfer in partially cloudy atmosphere, J. Atmos. Sci. **50**, 2146 (1993).

[13] V. E. Zuev and G. A. Titov, Radiative transfer in cloud fields with random geometry, J. Atmos. Sci. **52**, 176 (1995).

[14] N. Byrne, 3D radiative transfer in stochastic media, *3D Radiative Transfer in Cloudy Atmospheres*, edited by A. Marshak and A. Davis (Springer, Berlin, 2005), pp. 385–424.

[15] Y. Gu, C. Lindsey, and J. T. Jefferies, Radiative transfer in stochastic media, Astrophys. J. **450**, 318 (1995).

[16] G. C. Pomraning, Radiative transfer and transport phenomena in stochastic media, Int. J. Eng. Sci. **36**, 1595 (1998).

[17] E. Kassianov and D. Veron, Stochastic radiative transfer in Markovian mixtures: Past, present, and future, J. Quant. Spectrosc. Radiat. Transfer **112**, 566 (2011).

[18] G. C. Pomraning, *Linear Kinetic Theory and Particle Transport in Stochastic Mixtures* (World Scientific, Singapore, 1991), Vol. 7.

[19] S. Chandrasekhar, *Radiative Transfer* (Dover, New York, 1960).

[20] J. C. J. Paasschens, Solution of the time-dependent Boltzmann equation, Phys. Rev. E **56**, 1135 (1997).

[21] C. D. Levermore, G. C. Pomraning, D. L. Sanzo, and J. Wong, Linear transport theory in a random medium, J. Math. Phys. **27**, 2526 (1986).

[22] D. Vanderhaegen, Radiative transfer in statistically heterogeneous mixtures, J. Quant. Spectrosc. Radiat. Transfer **36**, 557 (1986).

[23] G. C. Pomraning, Radiative transfer in random media with scattering, J. Quant. Spectrosc. Radiat. Transfer **40**, 479 (1988).

[24] M. L. Adams, E. W. Larsen, and G. C. Pomraning, Benchmark results for particle transport in a binary Markov statistical medium, J. Quant. Spectrosc. Radiat. Transfer **42**, 253 (1989).

[25] C. Deutsch and D. Vanderhaegen, Radiative transfer in statistically heterogeneous mixtures, J. Quant. Spectrosc. Radiat. Transfer **44**, 163 (1990).

[26] B. Su and G. C. Pomraning, Benchmark results for particle transport in binary non-Markovian mixtures, J. Quant. Spectrosc. Radiat. Transfer **50**, 211 (1993).

[27] O. Zuchuat, R. Sanchez, I. Zmijarevic, and F. Malvagi, Transport in renewal statistical media: Benchmarking and comparison with models, J. Quant. Spectrosc. Radiat. Transfer **51**, 689 (1994).

[28] O. Haran, D. Shvarts, and R. Thieberger, Transport in two-dimensional scattering stochastic media: Simulations and models, Phys. Rev. E **61**, 6183 (2000).

[29] P. S. Brantley, A benchmark comparison of Monte Carlo particle transport algorithms for binary stochastic mixtures, J. Quant. Spectrosc. Radiat. Transfer **112**, 599 (2011).

[30] E. W. Larsen and R. Vasques, A generalized linear Boltzmann equation for non-classical particle transport, J. Quant. Spectrosc. Radiat. Transfer **112**, 619 (2011).

[31] C.-Z. Gao, C.-B. Zhang, C.-X. Yu, X.-F. Xu, S.-C. Wang, C. Yang, Z.-Y. Hong, Z.-F. Fan, and P. Wang, Stochastic radiative transfer in random media: Pure absorbing cases, Phys. Rev. E **102**, 022111 (2020).

[32] C. Larmier, F.-X. Hugot, F. Malvagi, A. Mazzolo, and A. Zoia, Benchmark solutions for transport in *d*-dimensional Markov binary mixtures, J. Quant. Spectrosc. Radiat. Transfer **189**, 133 (2017).

[33] C. Larmier, A. Zoia, F. Malvagi, E. Dumonteil, and A. Mazzolo, Monte Carlo particle transport in random media: The effects of mixing statistics, J. Quant. Spectrosc. Radiat. Transfer **196**, 270 (2017).

[34] C. Larmier, A. Lam, P. Brantley, F. Malvagi, T. Palmer, and A. Zoia, Monte Carlo chord length sampling for *d*-dimensional Markov binary mixtures, J. Quant. Spectrosc. Radiat. Transfer **204**, 256 (2018).

[35] S. P. Regan, R. Epstein, B. A. Hammel, L. J. Suter, H. A. Scott, M. A. Barrios, D. K. Bradley, D. A. Callahan, C. Cerjan, G. W. Collins, S. N. Dixit, T. Döppner, M. J. Edwards, D. R. Farley, K. B. Fournier, S. Glenn, S. H. Glenzer, I. E. Golovkin, S. W. Haan, A. Hamza *et al.*, Hot-Spot Mix in Ignition-Scale Inertial Confinement Fusion Targets, Phys. Rev. Lett. **111**, 045001 (2013).

[36] B. Bachmann, J. E. Ralph, A. B. Zylstra, S. A. MacLaren, T. Döppner, D. O. Gericke, G. W. Collins, O. A. Hurricane, T. Ma, J. R. Rygg, H. A. Scott, S. A. Yi, and P. K. Patel, Localized mix-induced radiative cooling in a capsule implosion at the National Ignition Facility, Phys. Rev. E **101**, 033205 (2020).

[37] A. Pak, L. Divol, C. R. Weber, L. F. B. Hopkins, D. S. Clark, E. L. Dewald, D. N. Fittinghoff, V. Geppert-Kleinrath, M. Hohenberger, S. Le Pape, T. Ma, A. G. MacPhee, D. A. Mariscal, E. Marley, A. S. Moore, L. A. Pickworth, P. L. Volegov, C. Wilde, O. A. Hurricane, and P. K. Patel, Impact of Localized Radiative Loss on Inertial Confinement Fusion Implosions, Phys. Rev. Lett. **124**, 145001 (2020).

[38] D. S. Miller, F. Graziani, and G. Rodrigue, Benchmarks and models for time-dependent grey radiation transport with material temperature in binary stochastic media, J. Quant. Spectrosc. Radiat. Transfer **70**, 115 (2001).

[39] B. Su and G. C. Pomraning, Limiting correlation length solutions in stochastic radiative transfer, J. Quant. Spectrosc. Radiat. Transfer **51**, 893 (1994).

[40] A. K. Prinja and G. L. Olson, Grey radiative transfer in binary statistical media with material temperature coupling: Asymptotic limits, J. Quant. Spectrosc. Radiat. Transfer **90**, 131 (2005).

[41] G. L. Olson, Gray radiation transport in multi-dimensional stochastic binary media with material temperature coupling, J. Quant. Spectrosc. Radiat. Transfer **104**, 86 (2007).

[42] G. L. Olson, Grey and multigroup radiation transport models for two-dimensional stochastic media with material temperature coupling, J. Quant. Spectrosc. Radiat. Transfer **113**, 325 (2012).

[43] G. L. Olson, Gray and multigroup radiation transport models for two-dimensional binary stochastic media using effective opacities, J. Quant. Spectrosc. Radiat. Transfer **168**, 57 (2016).

[44] G. L. Olson, Gray and multigroup radiation transport through 3D binary stochastic media with different sphere radii distributions, J. Quant. Spectrosc. Radiat. Transfer **189**, 243 (2017).

[45] P. S. Brantley, N. A. Gentile, and G. B. Zimmerman, A Levermore-Pomraning algorithm for implicit Monte Carlo radiative transfer in binary stochastic media, Trans. Am. Nucl. Soc. **105**, 498 (2011).

[46] P. Brantley, N. Gentile, and G. Zimmerman, Beyond Levermore-Pomraning for implicit Monte Carlo radiative transfer in binary stochastic media, Lawrence Livermore National Laboratory report, LLNL-CONF-724017, 2017.

[47] P. S. Brantley and G. B. Zimmerman, Benchmark comparison of Monte Carlo algorithms for three-dimensional binary stochastic media, Lawrence Livermore National Laboratory report, LLNL-CONF-733467, 2017.

[48] P. Brantley and J. Martos, Impact of spherical inclusion mean chord length and radius distribution on three-dimensional binary stochastic medium particle transport, Lawrence Livermore National Laboratory, LLNL-CONF-472011, 2011.

[49] G. C. Pomraning, *The Equations of Radiation Hydrodynamics* (Pergamon, Oxford, 1973).

[50] D. Mihalas and B. W. Mihalas, *Foundations of Radiation Hydrodynamics* (Oxford University Press, Oxford, 1984).

[51] B. Su and G. L. Olson, An analytical benchmark for non-equilibrium radiative transfer in an isotropically scattering medium, Ann. Nucl. Energy **24**, 1035 (1997).

[52] C.-Z. Gao, Y. Cai, and Z.-F. Fan, RAREBIT1D: Radiative transfer in binary stochastic mixtures for planar, spherical, and cylindrical geometries in one dimension (unpublished).

[53] See Supplemental Material at http://link.aps.org/supplemental/10.1103/PhysRevE.105.014131 for more numerical details involved in this study, including the validation of the discretization strategy, the verification of energy conservation, and the definition of channel-resolved radiation flux.

[54] C. D. Levermore, J. Wong, and G. C. Pomraning, Renewal theory for transport processes in binary statistical mixtures, J. Math. Phys. **29**, 995 (1988).

[55] J. J. Duderstadt and W. R. Martin, *Transport Theory* (Wiley-Interscience, New York, 1979).

[56] A. P. Roberts, Statistical reconstruction of three-dimensional porous media from two-dimensional images, Phys. Rev. E **56**, 3203 (1997).

[57] C. L. Y. Yeong and S. Torquato, Reconstructing random media, Phys. Rev. E **57**, 495 (1998).

[58] M. L. Adams and E. W. Larsen, Fast iterative methods for discrete-ordinates particle transport calculations, Prog. Nucl. Energy **40**, 3 (2002).

[59] C. Larmier, E. Dumonteil, F. Malvagi, A. Mazzolo, and A. Zoia, Finite-size effects and percolation properties of Poisson geometries, Phys. Rev. E **94**, 012130 (2016).